Development and Implementation of a New Solid-State Battery Testing Tool

Undergraduate Honors Thesis

Presented in Partial Fulfillment of the Requirements for Graduation with Honors Distinction in the Department of Mechanical Engineering at The Ohio State University

Christian Wengerter

April 2020

Advisor: Jung-Hyun Kim, Ph.D.

Abstract:

Since lithium-ion batteries have become the sought-after battery in today's market, they can be found in many devices we use every day such as cell phones, laptops, and electric vehicles. One major issue with this advancement is that there has not been much progression in the cell design of all solid-state batteries. Therefore, I propose to design a new solid-state battery cell that will facilitate electrochemical reaction between electrodes and solid electrolyte by allowing high pressure and heat to be externally applied. In addition, the new cell design will need to maintain a gas-tight seal around the components to allow researchers the ability to test air sensitive materials. My goal is to produce a design that will outperform the current commercial solid-state battery cell, while maintaining a smaller design for more practical laboratory use. In particular, the aim of mechanical design is to achieve a pressure on the battery components that is larger than 20 MPa. This high pressure would be exerted by a hydraulic press once the three compounds have been placed in the battery cell. After repeated mechanical designs and fabrication of a prototype, 303 MPa could be achieved on the battery components while heating to 200°C and confirming an air-tight sealing of the cell. The new cell is also more compact with a decrease in dimensions by approximately 30%, making use easier inside of an Argon-filled glovebox. In addition, the proper quantity of composite $LiNbO_3$-$LiCoO_2$ cathode, $Li_{10}GeP_2S_{12}$ electrolyte, and indium anode has been identified to build a functional cell. The tooling can also facilitate better heat transfer to the battery compounds while also achieving a higher working temperature. The results have shown that using 303 MPa on the battery compounds while applying 200°C for 45 minutes, can achieve an open circuit voltage of 3.6 volts vs LiIn/Li^+ and a specific capacity of 100 g/mAh.

Acknowledgements:

There are many individuals who have provided guidance and support throughout my undergraduate research project. First off, I would like to thank Dr. Kim, my research advisor, who has been pivotal in helping me accomplish my goals. Dr. Kim provided me with any resource that was needed, along with valuable advice and support. Before developing my proposal, Dr. Kim started a battery crash course in which myself, Dr. Kim, and a few undergraduate students met once a week, for 10 weeks, in order to learn the background of batteries and how to better implement our research topics. The crash course was very beneficial in helping me better understand electrochemistry in order to make a tool to facilitate the chemical reaction. Even though our schedules did not always line up, Dr. Kim was very flexible which allowed for important input in the various stages of the project.

Secondly, I would like to thank Chanyeop Yu, a graduate student who also works in the Energy Innovation Lab. Chanyeop was like a second advisor and his support was critical in helping me with test setups and evaluating experimental results. In addition, he provided me with a litany of background research that helped guide my design parameters throughout the project.

During the design and manufacturing stages, I had help from outside my research lab as well. Kevin Wolf and Chad Bivens in the Ohio State prototyping machine shop in Scott Laboratories helped me tremendously with questions about dimensioning and machining and helped me laser cut customs gaskets. After finalizing my design, I was ready to begin machining it myself. Aaron Orsborn was instrumental in troubleshooting machining issues and facilitating the use of the machines in the student machine shop.

Table of Contents:

Table of Figures:

Table of Charts:

Chapter 1: Introduction

Before designing a tool to test lithium-ion batteries, it is important to understand what they are and how they work. Lithium-ion batteries consist of a positive electrode, a negative electrode, and an ionically conductive electrolyte. The positive electrode is referred to as the cathode, the negative as the anode, and the electrolyte is found in between the electrodes which facilitates the ion transfer between them. Lithium-ion batteries are classified as secondary batteries meaning they can be recharged [1]. During charging, ions from the cathode move through the electrolyte to the anode. Then, during discharging, the ions move back to the cathode producing a flow of electrons, producing a current and voltage which can be used to power other devices. Lithium-ion batteries can maintain an average discharge of 3.7 volts vs Li^-/Li^+, which is high among current batteries, and are one of the most lightweight batteries due to having the highest energy density of all currently available batteries [1]. Figure 1 below gives an accurate representation of how lithium-ion batteries are constructed. The green dots represent the ions which are transferred back and forth through the electrolyte.

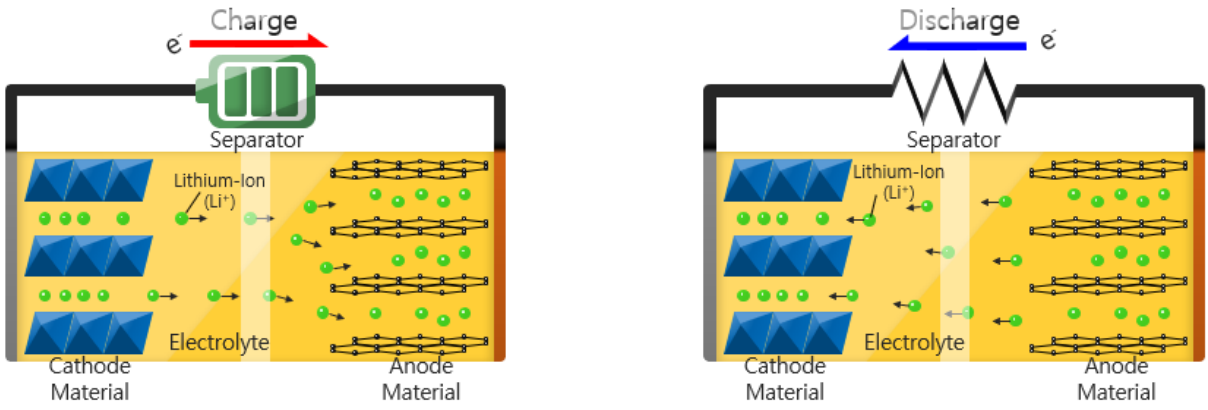

Figure 1: Lithium-Ion battery schematic (courtesy of Chanyeop Yu for figure)

With lithium-ion batteries having a large voltage output and the highest energy density, they have been utilized in larger scale applications such as in electric vehicles. The downside to increasing the size of the batteries is that the amount of flammable organic liquid electrolyte also increases [2]. The increase in flammable electrolyte produces a safety hazard, especially in an automobile accident. Since the solid-state lithium-ion batteries use non-flammable ceramic material, the solid-state batteries are completely free from firing issues. Thanks to the safety of the batteries, numerous research groups, including academic and industrial, have intensively investigated solid-state lithium-ion batteries [1-12].

The difference between the liquid electrolyte and the solid electrolyte is that the ions must transfer through a solid instead of a liquid making it harder to produce a high conductivity. Figure 2 [3] displays the comparison of a conventional battery with a liquid electrolyte on the left, and a solid-state battery with solid electrolyte on the right.

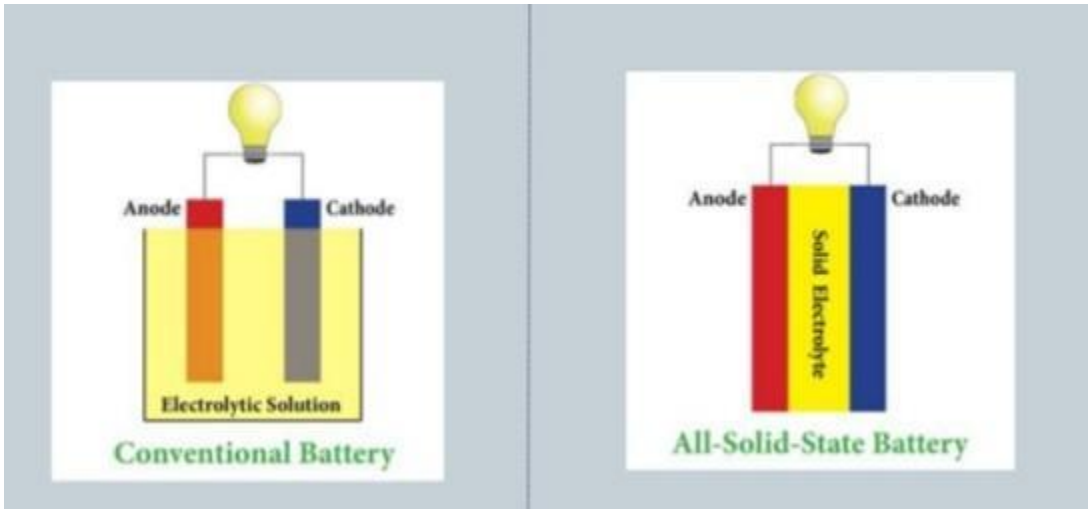

Figure 2: Conventional battery vs Solid-State battery [3]

Conductivity is produced in the solid electrolyte when ions move through vacancies or interstitials in the electrolyte when transferring between the cathode and anode [4], as seen in Figure 3 below. The cathode and anode are the same structure as in liquid electrolyte batteries, which is in a powder form. When using a liquid electrolyte, it is easy to ensure that the ions will be able to move easily since the liquid is able to fill the container and thus touch every part of the cathode and anode producing a high conductivity.

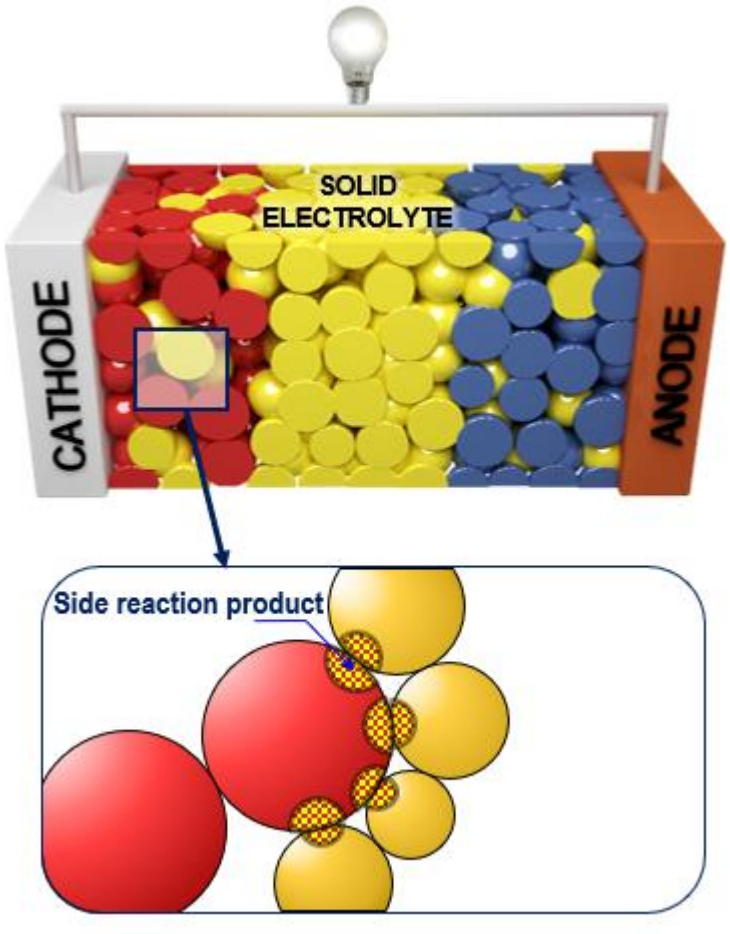

Figure 3: Demonstration of solid electrolyte interface with the cathode and anode (courtesy of Chanyeop Yu for figure)

The obstacle in designing a tool to test the solid-state battery is that there needs to be enough pressure to force the cathode and anode to touch as much of the solid electrolyte as possible. The current commercial tool that is used at Nano Tech West, provided by MTI Corporation, has a maximum allowable pressure of 20 MPa. This parameter will be the baseline goal of designing a tool with a much larger pressure range. Another key aspect of designing a new tool is that external heat may need to be applied to help increase the density of the solid electrolyte. With the addition of external heat, the anode and cathode can be softened enough to allow for maximum surface contact between the 3 battery components. Since the components must be held in a nonconductive material, a thermoplastic is one of the best candidates due to its high melting temperatures. Since the glass transition temperature of PEEK is roughly 143°C, this temperature will be a good maximum metric to plan for so that the PEEK plastic does not begin to lose its physical properties. Then, a conductive metal will need to be used to touch the cathode to create the positive lead and another piece of conductive metal will be used to touch the anode to create the negative lead. This research is being driven by the need for a better understanding of how solid electrolytes function under different external parameters and how to achieve similar performances to that of conventional batteries with liquid electrolytes. The new tooling and exploration of how the tool interacts with the battery materials will help future researchers implement solid-state batteries into commercial use.

1.1 Focus of Thesis

The purpose of this research project is to develop a more versatile tool to be implemented into the testing of solid electrolytes and learn more about how these tools can be optimized to

achieve the best battery performances. To develop the new design, the current tool used at Nano Tech West was used as a benchmark which can be seen in Figure 4 below [5].

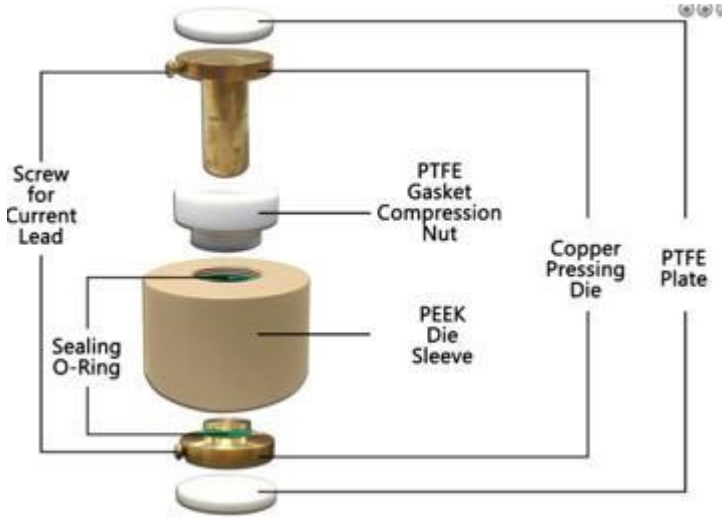

Figure 4: Current commercial tool used at Nano Tech West [5]

With the three main design requirements being external pressure, external heat, and an air-tight seal, I used SolidWorks CAD modeler to brainstorm different design ideas to achieve these design requirements. To help narrow down design ideas, I used SolidWorks built in FEM simulator to see where the stress concentrations would occur in the different designs. After deciding on a final design, I fabricated the design and moved to testing and validation. To test and validate the new tool design, $Li_{10}GeP_2S_{12}$ (LGPS) was selected [2] as the solid electrolyte. By using this electrolyte, the air-tight seal also needs to be maintained as the sulfur in the LGPS can interact with air and create H_2S gas. In addition, $LiNbO_3$-$LiCoO_2$ has been used for the cathode material and indium has been chosen as the anode. By using different quantities of the battery materials and different external factors, I investigated the open circuit voltage vs the specific capacity by cycling the

battery for more than one cycle. By using the electrochemistry results, the parameters of the test could be changed to try to achieve improved performance.

1.2 Significance of Research

The environmental state of the world is becoming an increasing focal point, with many man-made things contributing to dangerous byproducts which can harm the environment. One major byproduct is the burning of gasoline in vehicles as CO_2 is a dangerous greenhouse gas that eats away at the ozone layers within the earth's atmosphere. Because of how many vehicles are on the road, there has been a push for alternate green energy sources such as using batteries in vehicles to reduce the amount of gasoline burned. Electricity can also be a renewable resource which could, in turn, be a better alternative to gasoline for long term sustainability in terms of it being less harmful to the earth. There are some promising electric vehicles on the market already. To power these vehicles, high-powered long-lasting lithium-ion batteries have been the sought-after choice.

With the implementation of lithium-ion batteries in vehicles, there is an environmental benefit but also a benefit to those driving the vehicles. Gasoline engines need a reservoir of gasoline in the vehicle. This combination can prove to be dangerous if, in the event of an accident, the gasoline catches fire thus engulfing the vehicle in flames. Lithium-ion batteries replace the gasoline in the vehicles reducing the likelihood of the vehicle catching fire as a result of an accident or malfunction. Unfortunately, the safety hazard has not been completely removed yet. Conventional lithium-ion batteries use a liquid electrolyte which is an organic material that is still very flammable. Although the substitution of the battery for a gasoline engine solves many problems, it still presents safety issues if the battery short circuits or is damaged in an automobile accident.

My research is driven by the need to completely remove the safety issue, which can be accomplished by substituting the conventional battery with the solid-state battery. As mentioned in the introduction, the solid electrolytes within the solid-state battery are inorganic non-flammable materials. A concern is that although these LGPS and other electrolytes have been studied there is still some controversy around them. Added external pressure and heat can be more investigated to see how this benefits the ionic transfer within the electrolyte. In order to make this substitution of a solid-state battery for a conventional battery, the specific capacity of the batteries and the voltage output must be comparable.

1.3 Overview of Thesis

This thesis paper has a total of 5 Chapters: Introduction, Experiments, Results, Discussion, Conclusion, and Future Work. In Chapter 2, I discuss the sample preparation of the cathode coating, the test procedure to validate the air-tight sealing, and the overarching test procedure for testing the solid electrolytes in the new tool. In Chapter 3, I discuss the design process and the results from the FEM simulations, heat transfer analysis, and fabrication. Additionally, I discuss the different parameters that were used in each test iteration and the results from each test. Lastly, I discuss my conclusions and final findings in Chapter 4, as well as my future recommendations for students and further research in Chapter 5.

Chapter 2: Experiments

2.1 Cathode Material Preparation

In order to passivate the LGPS/electrode interface, $LiCoO_2$ (LCO) cathode powder was coated with $LiNbO_3$. Lithium acetate and niobium ethoxide were mixed with a stoichiometric ratio

in an Argon-filled glovebox and dissolved in anhydrous ethanol. After making the solution-state, cathode material was added into the solution, and then mixed overnight. Ultra-sonication was applied to improve the dispersion of LCO particles in the solution. The obtained solution was dried overnight, followed by calcining at 300^{o}C for 12 hours to remove the remaining organic material. It was then re-heated at 400^{o}C for 5 minutes. The $LiNbO_3$ coating layer was confirmed through the SEM-EDX (Scanning Electron Microscope – Energy Dispersive X-Ray Spectroscopy) observation.

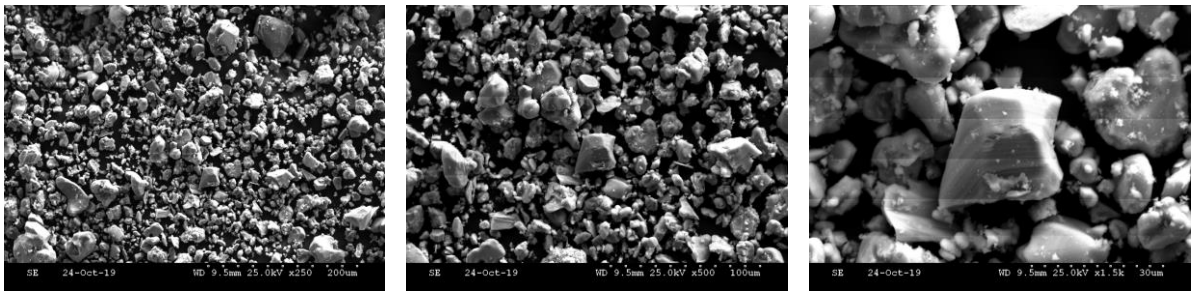
SE 24-Oct-19 WD 9.5mm 25.0kV x250 200um
SE 24-Oct-19 WD 9.5mm 25.0kV x500 100um
SE 24-Oct-19 WD 9.5mm 25.0kV x1.5k 30um

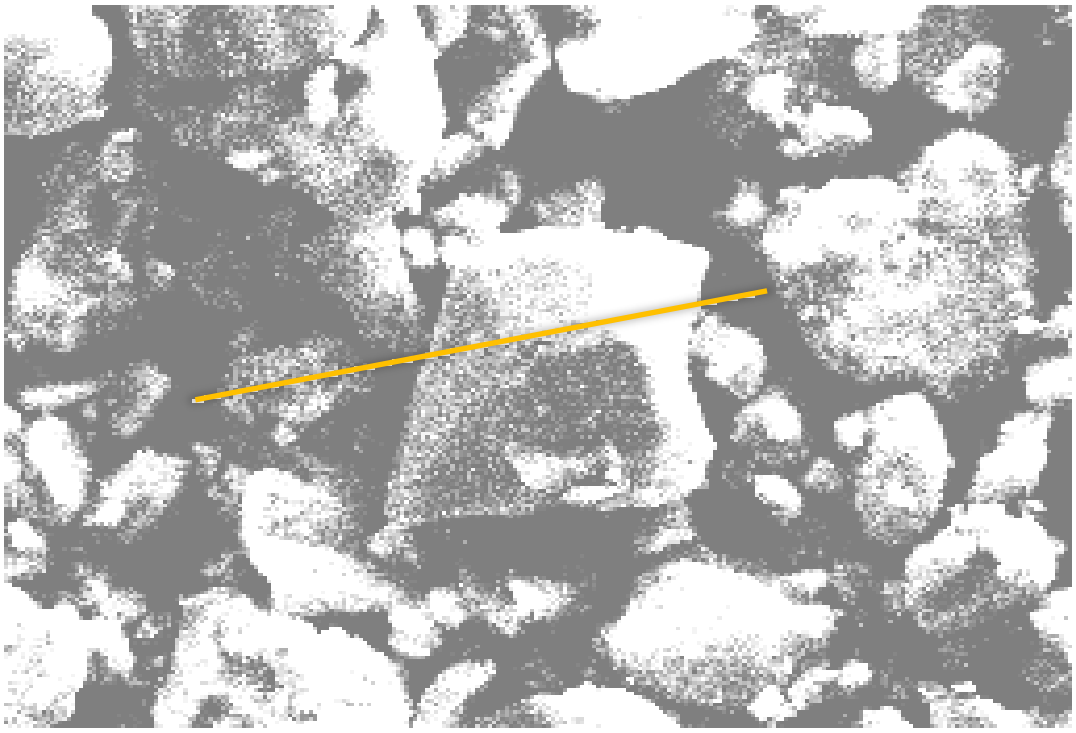

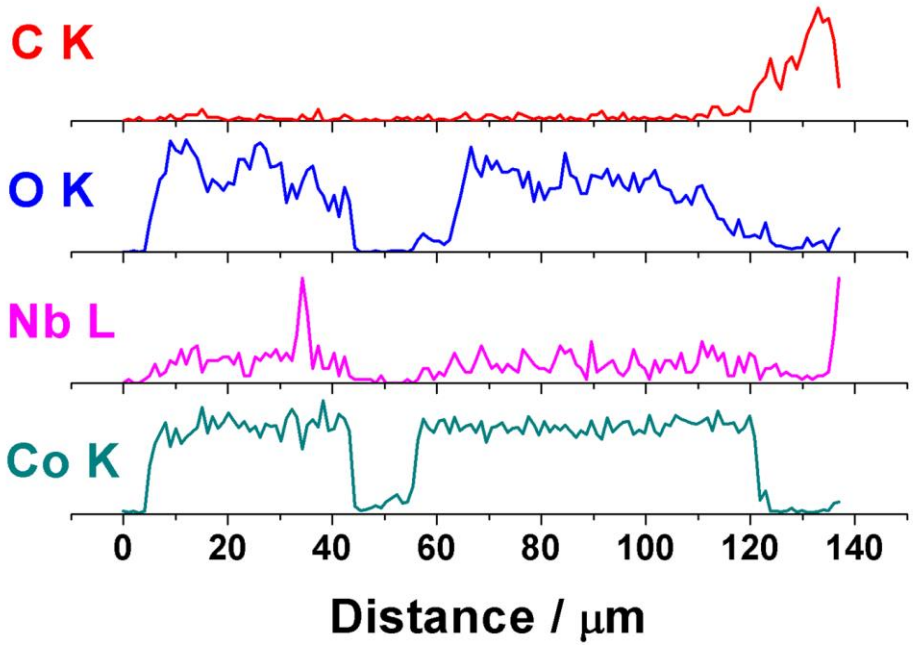
C K
O K
Nb L
Co K
0
20
40
60
80
100
120
140
Distance / μm

Figure 5: SEM-EDX images of $LiNbO_3$ coating on $LiCoO_2$. The normalized quantities of each element (C, O, Nb, and Co) were indexed along the yellow line. (courtesy of Chanyeop Yu for figure)

2.2 Air-Tight Seal Validation Test Procedure

The first test on the tool is to validate that the gasket and O-ring provide a good enough air-tight seal so that the LGPS, that will be tested in the tool, does not interact with air to produce H_2S gas. To begin the testing, the tool was inserted into an Argon-filled glovebox, as shown in Figure 6. Once the tool was in the air-controlled environment, the pure lithium metal could be inserted into the tool and reassembled together, as shown in Figure 11. The assembled tool was then removed from the air-controlled environment to be left out for 24 hours. At the end of the 24 hours, the tool was disassembled in the glovebox to investigate the lithium metal on the inside of the tool.

This test validates the tools air-tight sealing capabilities, as lithium metal is very reactive to air. When pure lithium metal interacts with air, it oxidizes which forms a dark matte gray color on its outer surface. The equations below demonstrate the two oxidation reactions that occur when pure lithium metal interacts with air.

$$6 * Li(s) + N_2(g) \rightarrow 2 * Li_3N(s)$$
$$4 * Li(s) + O_2(g) \rightarrow 2 * Li_2O(s)$$

2.3 Solid-State Battery Testing Procedure

The following will describe how the test setup was constructed and how the solid electrolytes are tested. The instructions provide the overarching methodology of how every test

was performed. Within each test, component amounts and external loadings were varied. These varying parameters will be discussed in the results and discussion section.

First, all the tools and equipment are placed inside of an Argon-filled glovebox, as shown in Figure 6. To begin testing, each part of the tool is cleaned using anhydrous ethanol to ensure that there is no residue from the previous testing that could skew results. The first material to be implemented into the tool will be the selected solid electrolyte LGPS. The compound is then weighed on an electronic scale, as shown in Figure 7, and the LGPS is poured into the top of the tool by removing the top plunger. The top plunger is placed back into the assembly and is set into the hydraulic press, as shown in Figure 8. A force is then applied to the battery compounds which is recorded using the pressure gauge readout. The first pressure that is applied on the LGPS is a low pressure which is used to essentially create a layer so that the cathode powder does not mix with the electrolyte powder. After pressing the LGPS for 10-15 minutes, the three-part composite cathode material ($LiNbO_3$-$LiCoO_2$, Carbon black, and LGPS) is weighed on the scale. The cathode materials are then mixed in a mortar and pestle for 10-15 minutes to produce a homogeneous compound. The bottom plunger is removed and the cathode powder is placed on the solid electrolyte layer. The bottom plunger is then placed back into the tool assembly and then back into the hydraulic press where it is pressed at the highest pressure for that test for an extended period of 30-45 minutes. If heat is incorporated into the test, it is utilized in this step by wrapping the tool assembly in heating bands, as shown in Figure 9. To measure the temperature, an infrared camera is used before and after the heating bands are applied.

After the pressure and heat are applied to the cathode and solid electrolyte material, the tool is removed from the hydraulic press and set aside to cool down. While the tool is cooling

down, the anode (indium) is prepared using a half inch hole punch, as seen in Figure 10. The top plunger is removed and the indium metal is placed on the LGPS layer. The tool is reassembled and placed back in the hydraulic press for one last low pressure loading which is applied for a short period of time such as 1-5 minutes. Now, the solid-state battery is assembled and ready for testing. The tool is placed in a secondary pressure apparatus that is provided by MTI Corp. Refer to Figure 11 for the setup. A positive lead is attached to the bottom plunger and the negative lead is attached to the top plunger for cycling. Current is sent into the battery using a VMP-3 cycling machine, then the battery is charged and discharged at the cycle rate set on EC-Lab software. The cycle rate that was chosen was C/100-rate or C/50-rate for the first cycle and C/20-rate for the subsequent cycles. C/100-rate stands for 100 hours for 1 cycle, C/50-rate stands for 50 hours per cycle, and C/20- rate stands for 20 hours per cycle. The open circuit voltage and specific capacity for each cycle are then outputted on the EC-Lab software for analysis.

Figure 6: Dual Argon-filled glovebox

Figure 7: Measuring LGPS on electronic scale

Figure 8: Tool assembly setup in the hydraulic press

Figure 9: Heating band setup in the hydraulic press

Figure 10: Half inch hole punch cutting indium metal foil

Figure 11: Battery tool in secondary pressure apparatus

Chapter 3: Results and Discussion

To begin this research project, parameters and metrics needed to be developed to design around. The goal is to design a tool that is very versatile in order to allow for a variety of test parameters to be applied on the solid electrolytes. To design a versatile tool, I used the pressure controlled split cell provided by MTI Corporation, as shown in Figure 4, as a benchmarking tool. The key parameters that I focused on were a) improving the external heat and pressure that could be applied without breaking the tool, b) maintaining an air-tight seal around the components, and c) reducing the size of the tooling to make it easier for other researchers to use it in a glovebox. MTI Corporation rated their tool for up to 20 MPa with a maximum working temperature of

80℃. But, the glass transition temperature of the PEEK plastic is around 143℃ and due to this I have aimed to make the maximum working temperature around 200℃. These two metrics, plus the other two stated above, were the driving design parameters when beginning the project.

I first started the design process by drawing out different ideas on paper and then took these designs to Dr. Kim or Chanyeop Yu to discuss the advantages and disadvantages of the designs. After many design iterations, some of which were completely different from MTI and some of which were similar, it became apparent that it may be better to modify an existing design instead of developing a completely different concept. I focused on the benchmarking tool and how to improve it to fulfill the design parameters. I eventually came up with a design that was appealing to myself, Dr. Kim, and Chanyeop. From there, I began modeling the design in SolidWorks CAD software. The design can be seen in Figures 12&13 below.

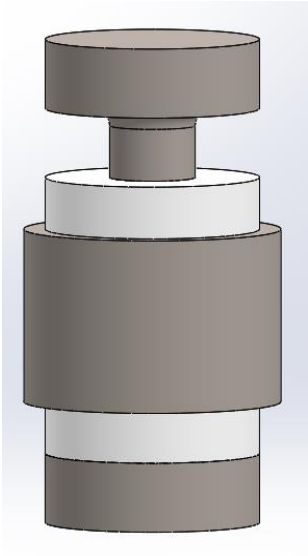

Figure 12: Fully assembled SolidWorks model of final design

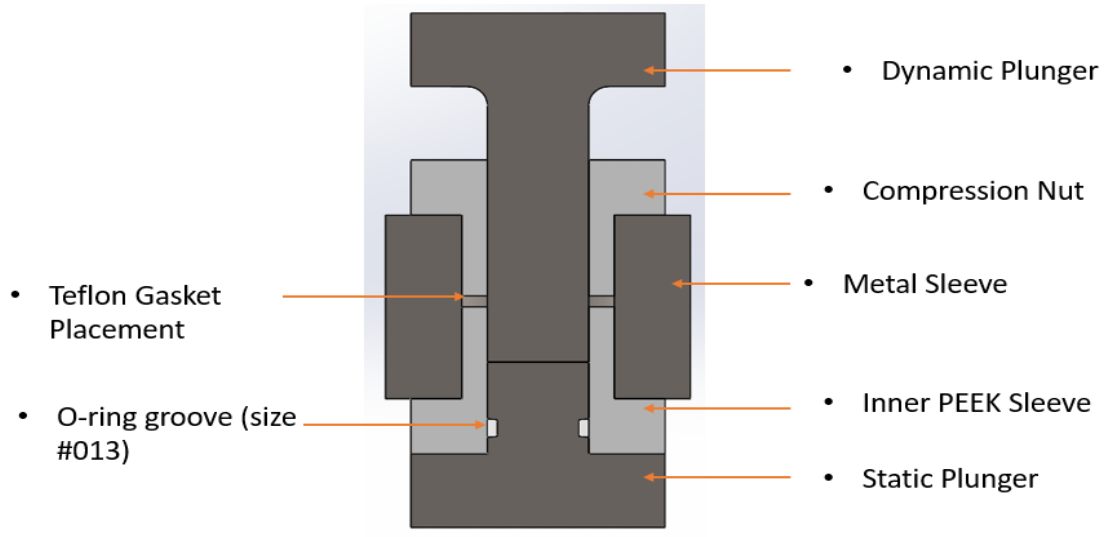

Figure 13: Fully assembled SolidWorks section view of final design

The gray pieces in Figures 12&13 represent 440c stainless steel, while the white pieces represent PEEK plastic or Polyether-ether-ketone. The gaps in Figure 13 are the locations in which the air-tight seal will be implemented. The gap between the two PEEK parts is for a custom-made Teflon gasket, 1/16 inch thickness, 0.497 inch inner diameter, and 0.74 inch outer diameter. The #013 imperial size O-ring groove on the static plunger is for a #011 imperial size O-ring. The detailed drawings of each part can be found in Appendix A. The drawings display the dimensions that were used, but to compare the size reduction from the MTI tool to the new tool please reference Table 1 below.

	Outermost diameter inch(mm)	Total length of assembly inch(mm)
MTI tool	2.17(55)	3.93(100)
New tool	1.5(38.1)	2.80(71.12)

Table 1: Size comparison between the benchmarking tool and the new tool

After developing the design in SolidWorks, I wanted to validate the tools rigidity by utilizing FEM (finite element methods) static stress simulations through SolidWorks add-ins. The goal was to ensure that the design assembly could withstand the 20 MPa before spending the time and money on fabrication of the tool. I assumed that 20 MPa was being exerted on the top of the dynamic plunger. The bottom of the assembly (i.e. static plunger) was fixed, meaning it could not move in the XYZ coordinate planes. I applied the material properties of the PEEK plastic and 440c stainless steel to the appropriate parts and ran the simulation. The results can be observed in Figure 14 below.

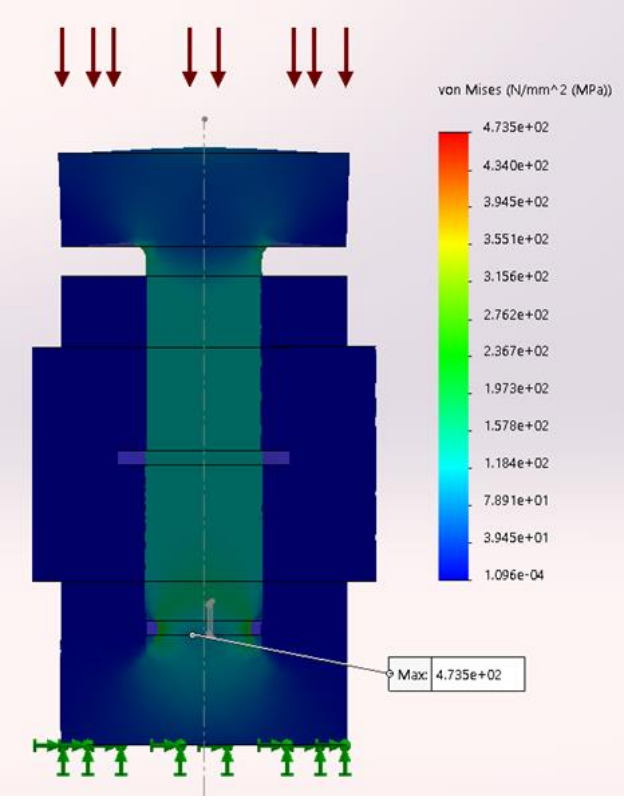

Figure 14: FEM results from static pressure simulation

The results showed that there would be a maximum stress of 473.5 MPa propagated on the O-ring groove on the static plunger. This was the expected site for the maximum Von-Mises stress, as the O-ring groove is a stress concentrator. The maximum stress is high, but the chosen stainless steel has a tensile strength of 785 MPa. From this, the max stress is slightly above half of the tensile strength and thus the tool is validated through simulation for the assumed parameters.

After validating the design, the next step was to develop drawings for fabrication, as shown in Appendix A. The three stainless steel parts were fabricated by the Smith Laboratories

machine shop given my limited expertise since these parts were very difficult to machine to tight tolerances. However, I was able to machine the two PEEK plastic parts myself on a Cincinnati Lathe in the Scott Laboratory student machine shop, with supervision from Aaron Orsborn. The finished parts are shown in Figures 15 & Figure 16 below.

Figure 15: Finished machined parts

Figure 16: Assembly of newly machined parts

To evaluate the new tool's heat conduction performance, I created a prototype PEEK sleeve. The test setup is shown in Figure 17. A thermometer was inserted into the 0.5 inch diameter hole while the heating bands were wrapped around the 1.5 inch outer diameter. The bands were then set to 200℃ and the internal temperature was recorded after 30 minutes and again when it reached steady-state. The results showed that the PEEK sleeve achieved an internal temperature of 125.5℃ after 30 minutes, and a steady-state temperature of 130℃ after 50 minutes. The wall thickness of the prototype was 0.5 inches and this was chosen because the total wall thickness of the new tool is 0.5 inches, with 0.375 inches of 440c stainless steel and 0.125 inch of PEEK plastic. With the incorporation of the metal sleeve, the heat conductivity is

improved compared to the all PEEK sleeve in the MTI tool with a wall thickness of 0.889 inches. 440c stainless steel has a thermal conductivity of ~24.2 W/mK [6], while PEEK plastic only has a thermal conductivity of ~0.29 W/mK [7]. With the higher conductivity of the stainless steel, the heat can penetrate to the battery material much faster than the full PEEK sleeve. Because the new tool has incorporated the stainless steel and reduced the PEEK plastic wall thickness, the new tool should be able to transmit heat faster than the 50 minutes from the test, and much quicker than the MTI tool with the thicker all PEEK sleeve. Additionally, the metal sleeve provides an added safety factor since the stainless steel tensile strength is much higher than PEEK plastic.

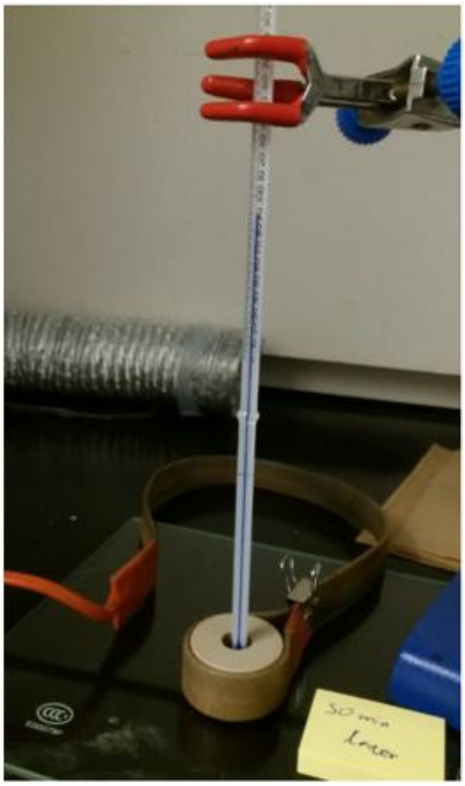

Figure 17: Test setup for the PEEK plastic sleeve prototype heating test

Before beginning testing of the cathode, anode, and solid electrolyte material, I first tested the air-tight sealing of the tooling. The process of the experiment can be found in Section 2.2. From this experiment, it was found that the tool could maintain an air-tight seal around the battery materials for at least 24 hours. The lithium metal in Figure 18 shows that it maintained its shiny surface and has not oxidized forming a dark matte gray surface. From this result, it has been determined that the air sensitive LGPS can be used in the tooling outside of the Argon-filled glovebox.

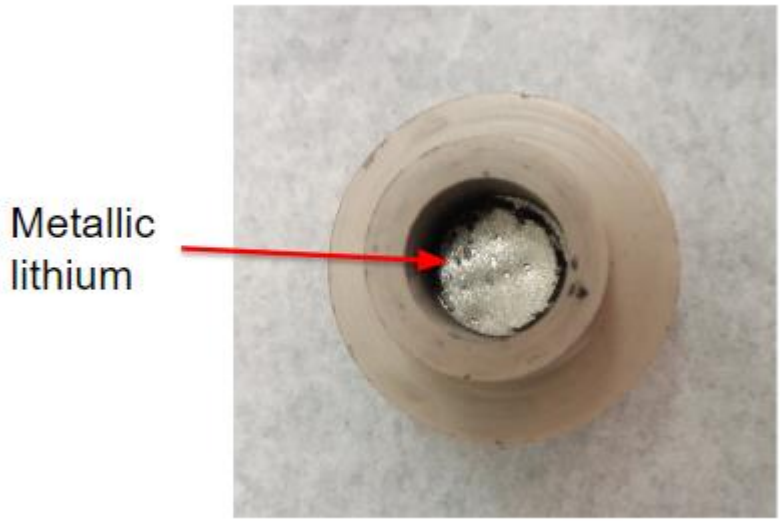

Figure 18: Photo of the shiny lithium metal in the testing tool after the tools sealing was exposed to air for 24-hrs

Section 2.3 can be used to reference the experimentation process used for testing the cathode, anode, and solid electrolyte material. Prior to these tests on the new tool, it was found that the current tool, provided by MTI in Figure 4, was breaking in the hydraulic press, as shown in Figure 19.

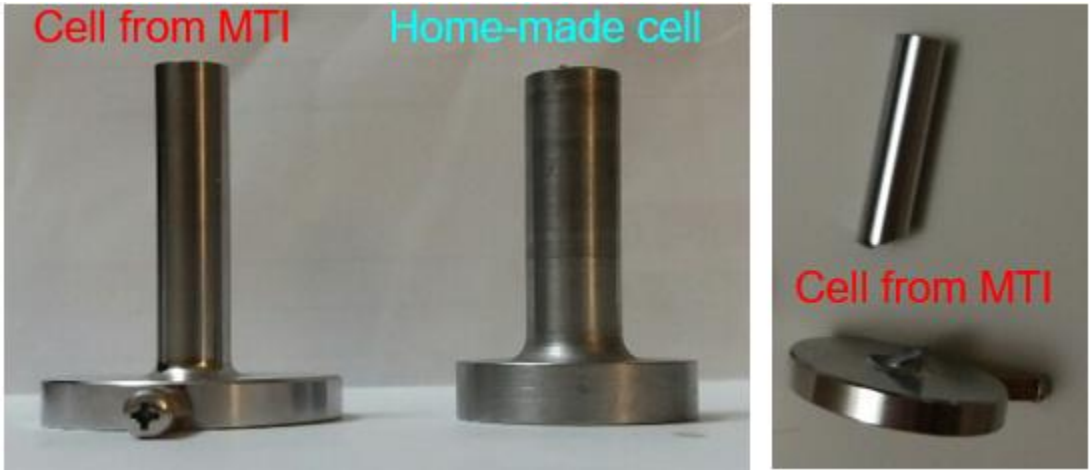

Figure 19: Demonstration of how MTI's tool has broken

The tool was rated for 20 MPa and was tested with less than this on the hydraulic pressure gauge readout. Due to the tool breaking, this led to an investigation of the MTI tool and the hydraulic press used. It was determined that the MTI tool was rated for 20 MPa on the smaller inner diameter (10 mm), not the larger diameter of the dynamic plunger that was used to base the FEM simulation on. After looking into the tool's performance, the hydraulic press was investigated to see how it was reading out its pressure. The diameter that the hydraulic press based its pressure readout on was a 70 mm hydraulic piston. Pressure is equal to $\frac{Force}{Area}$ and the area that the hydraulic press was using to base its pressure gauge readout on was much larger than the inner diameter of the MTI tool. The force is transmitted through the setup and with the area decreasing substantially it causes the tooling to break. From this, I wanted to develop a table to help researchers (as well as myself) to better understand the difference between the readout on the pressure gauge versus how much pressure is being pressed on the battery compounds. Table 2 below displays the pressure on the hydraulic press readout, the pressure on the battery compounds (with the new tool), the force being

transmitted, and the metric tons being produced. As shown in Table 2 below, by applying around 20 MPa on the hydraulic press, this corresponds to a very high force and thus higher pressure on battery compounds which was causing the MTI tool to break.

Pressure gauge reading (MPa): Hydraulic Press	Pressure on battery compounds (MPa): Half inch inner diameter	Force being produced (N)	Metric Tons
0.1	3.04	384.85	0.04
0.5	15.19	1924.23	0.20
1	30.38	3848.45	0.39
2	60.76	7696.90	0.78
3	91.14	11545.35	1.18
4	121.52	15393.80	1.57
5	151.90	19242.26	1.96
6	182.28	23090.71	2.35
7	212.66	26939.16	2.75
8	243.04	30787.61	3.14
9	273.42	34636.06	3.53
10	303.80	38484.51	3.92
11	334.18	42332.96	4.32
12	364.56	46181.41	4.71
13	394.94	50029.86	5.10
14	425.32	53878.31	5.49
15	455.70	57726.77	5.89
16	486.08	61575.22	6.28
17	516.46	65423.67	6.67
18	546.84	69272.12	7.06
19	577.22	73120.57	7.46
20	607.60	76969.02	7.85

Table 2: Pressure table for measurements

The equations used to develop Table 2 can be found in Appendix B along with a sample calculation. Using Table 2, I was able to prove that the new tool could support up to 303 MPa on the battery compounds compared to the 20 MPa on the MTI tool. This pressure could be held for 45 minutes while being heated at 200℃, compared to the tool that was used as a benchmark which could only be heated to 80℃. These pressure and heating values would then be used as the acceptable pressure and heating range of the tool to ensure that it would not break.

A factor that played a critical role in the new tool being able to withstand higher forces and pressure came from reducing the stress concentration factor K_t. As shown in Figure 20 [8], the ratio of $\frac{D}{d}$ and $\frac{r}{d}$ determine the stress concentration factor which correlates to how the maximum stress is calculated ($\sigma_{max} = \sigma_{avg} * K_t$). The new tool has decreased the diameter ratio from 4 (40 mm/10 mm) to 2.5 (1.25 in/0.5 in). Although this does decrease the stress concentration factor, the larger change comes from increasing the radius of the fillet in the new tooling, shown in Figure 19 above. As the ratio of $\frac{r}{d}$ increases the stress concentration decreases greatly. This change in dimension is critical to the design being able to withstand the large axial forces that will be placed on the plungers.

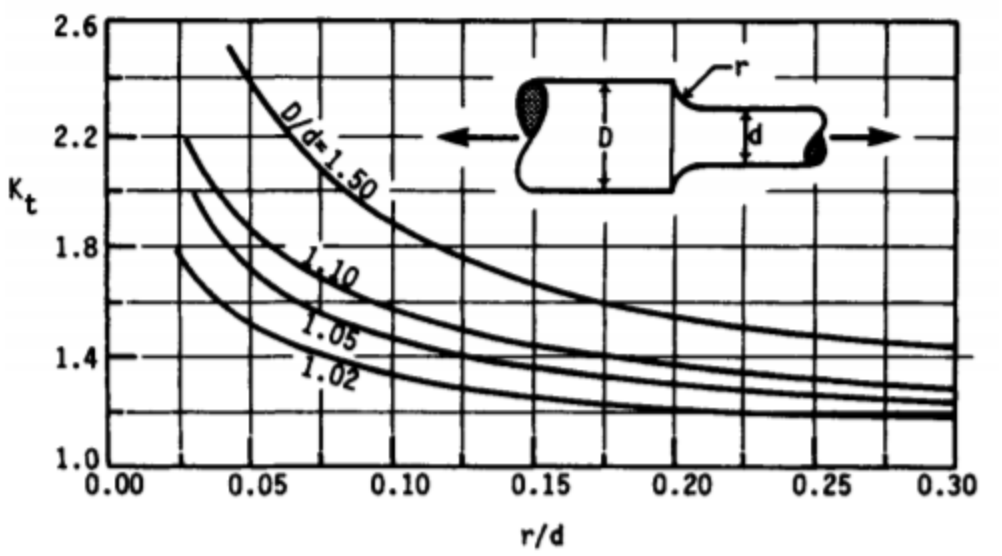

Figure 20:Stress concentration factor for a fillet under axial loading [8]

The results from the tests run on the new tooling can be seen in Table 5 (see page 34), while the setup conditions for each test shown in Tables 3 and 4. The first test had good results with a maximum open circuit voltage of around 3.6 volts vs LiIn/Li^+ and a specific capacity of around 90 g/mAh. The test only ran for one cycle before dropping in performance due to the increase in diameter where the battery compounds are located. The diameter changed from 10 mm to 12.7 mm. As a result, the cathode material could not cover the solid electrolyte as seen in Figure 21 below.

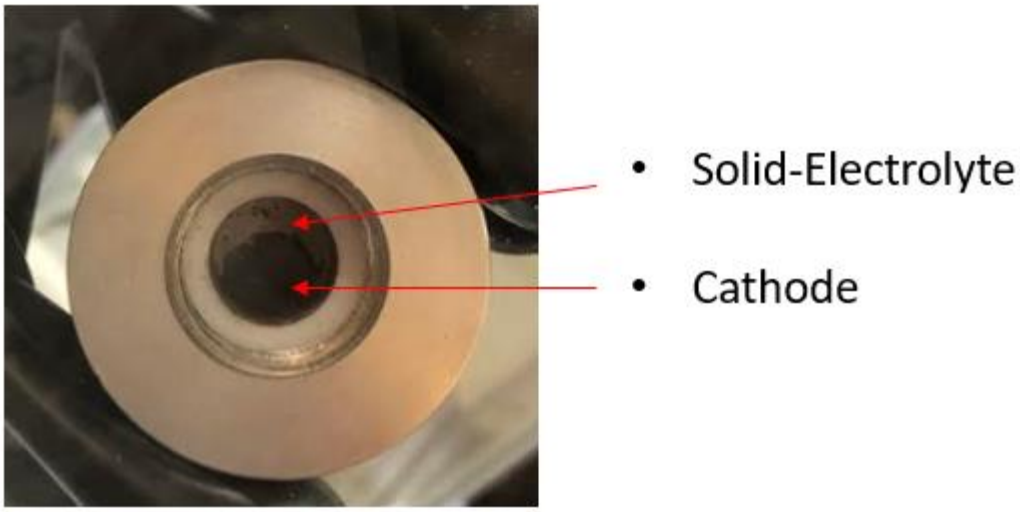

Figure 21: Cathode material failing to cover solid electrolyte

More cathode material was then added as shown in Table 3, but unfortunately the extra cathode material permeated through the solid electrolyte and caused the testing to short circuit, as shown Table 5. For test 3, the proper amount of battery compounds were inserted into the tooling. No heat treatment was done during the maximum pressure application of 150 MPa. The results showed that the maximum open circuit voltage stayed around 3.6 volts LiIn/Li^+, like in test one, and the specific capacity was around 85 g/mAh. The cyclability improved from the first test but is marginal as it dropped from 85 g/mAh to 25 g/mAh. To combat the poor cyclability, I decided to increase the maximum pressure on the battery compounds as well as add heat treatment to improve the conductivity between the three layers. The compounds were pressed at 303 MPa and heated at 200℃ for 45 minutes. The results showed that while the open circuit voltage remained about the same, the cyclability and specific capacity decreased. It was originally assumed that having higher pressure and higher heat would improve the interstitial sites between the electrolyte and the cathode material. These results showed otherwise, but to better characterize the setup I wanted to look at the cathode materials before making claims about the solid

electrolyte performance. In Figure 22 [9] shown below, a comparison of similar cathode materials was tested with solid electrolyte material and liquid electrolyte material.

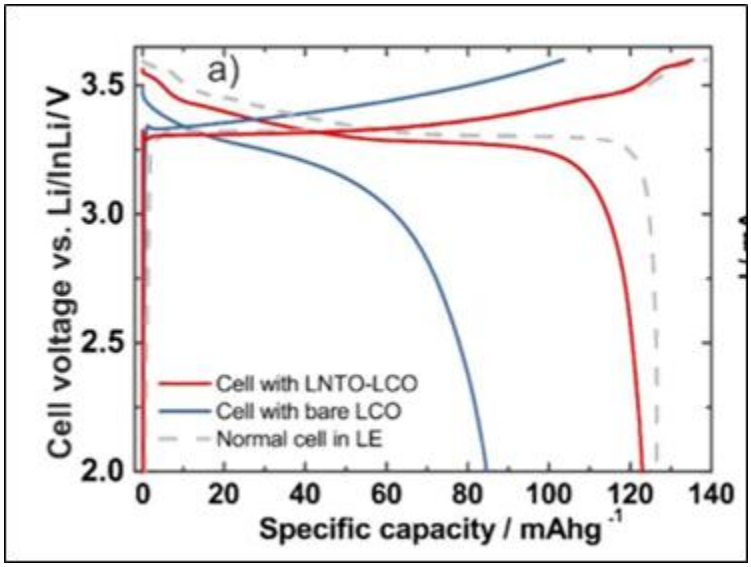

Figure 22: Comparison of different cathode coating materials on solid electrolyte and a normal cell in liquid electrolyte [9]

From the literature source, it was observed that as the cathode coating improved on the $LiCoO_2$ material, the specific capacity increased. This led to an investigation of the cathode coating that was implemented (see Section 2.1). In addition to the coating, carbon black and LGPS are added for conductivity. These three materials are combined by using a mortar and pestle for 10-15 minutes, but this may not be producing a homogeneous mixture between the compounds. With an insufficient homogenous mixture, the conductivity of the cathode can be reduced as the conductive materials will not be spread out properly thus increasing resistivity throughout the battery compounds. To combat the non-homogenous mixture, a roller mill can be used for a longer period than 10-15 minutes to prepare the material.

Figure 23 (see page 35) depicts the initial charge/discharge results for the $LiNbO_3$-coated $LiCoO_2$/$Li_{10}GeP_2S_{12}$/indium for test iterations 3-5. The fifth test iteration used the roller mill to prepare the cathode material, which was mixed for 24 hours. The other test parameters can be found in Tables 3&4. The results showed that the maximum open circuit voltage remained around 3.6 volts vs LiIn/Li^+, while the specific capacity increased from 75 g/mAh in test 4 to 100 g/mAh in test 5. The better mixing of the cathode material has improved the results for the first cycle, but due to the COVID-19 virus further testing on the cyclability of the battery from test 5 could not be evaluated. Further characterization of the battery compounds is needed to make claims about the correlation between external loadings and the battery performances. But, from the results shown, the correct amount of each battery compound found and the testing procedure laid out appropriately, the battery tool has been optimized for future testing. Future students will be able to characterize the battery compounds and test a variety of external loadings to present a correlation.

Test Iteration	Amount of Cathode Material 60:5:35 w% ($LiNbO_3$-coated $LiCoO_2$: Carbon Black: $Li_{10}GeP_2S_{12}$)	Amount of Solid electrolyte ($Li_{10}GeP_2S_{12}$)	Amount of Anode Material (indium metal)
1	20 mg	120 mg	½ inch coin
2	30 mg	120 mg	½ inch coin
3	40 mg	160 mg	½ inch coin
4	40 mg	160 mg	½ inch coin
5	40 mg	160 mg	½ inch coin

Table 3: Battery compound quantities for each test iteration

Test Iteration	Heat Treatment	Maximum Pressure on Battery Compounds	First Cycle Charging Rate (hours per cycle)	Subsequent Cycle Charging Rate (hours per cycle)	Mixing method for cathode materials
1	N/A	150 MPa	100	20	By hand
2	N/A	303 MPa	100	N/A	By hand
3	N/A	150 MPa	100	20	By hand
4	45 mins @200℃	303 MPa	50	20	By hand
5	45 mins @200℃	303 MPa	50	20	By Roll milling

Table 4: Test parameters for each test iteration

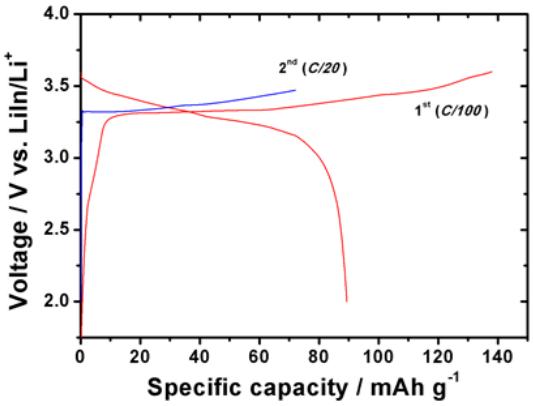

First Test

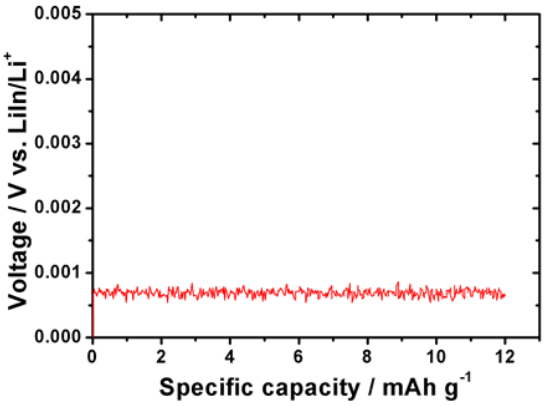

Second Test (Short-circuit)

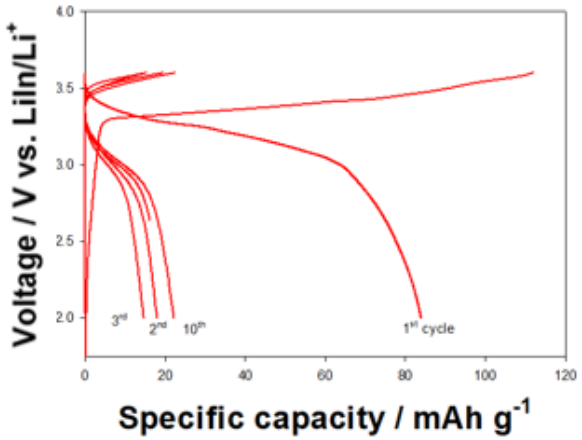

Third Test

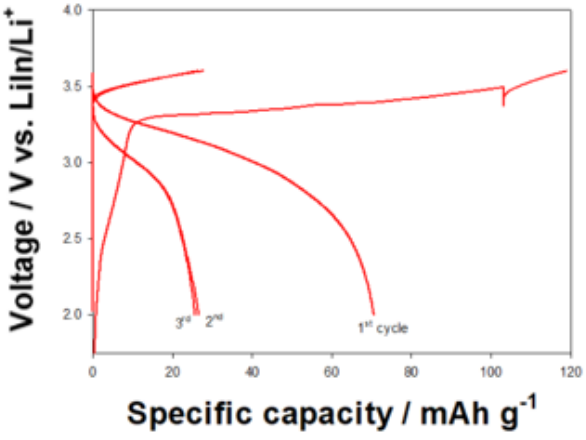

Fourth Test

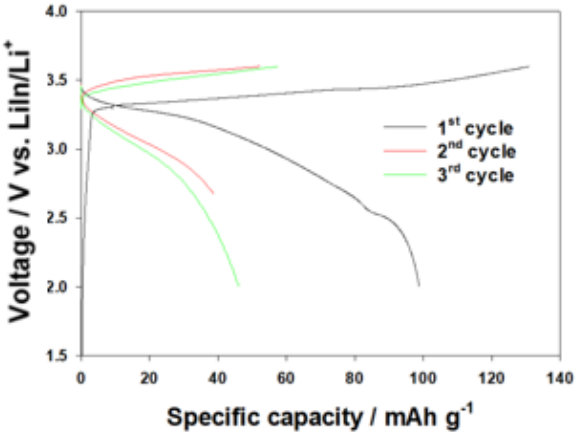

Fifth Test

Table 5: Test results from each test iteration

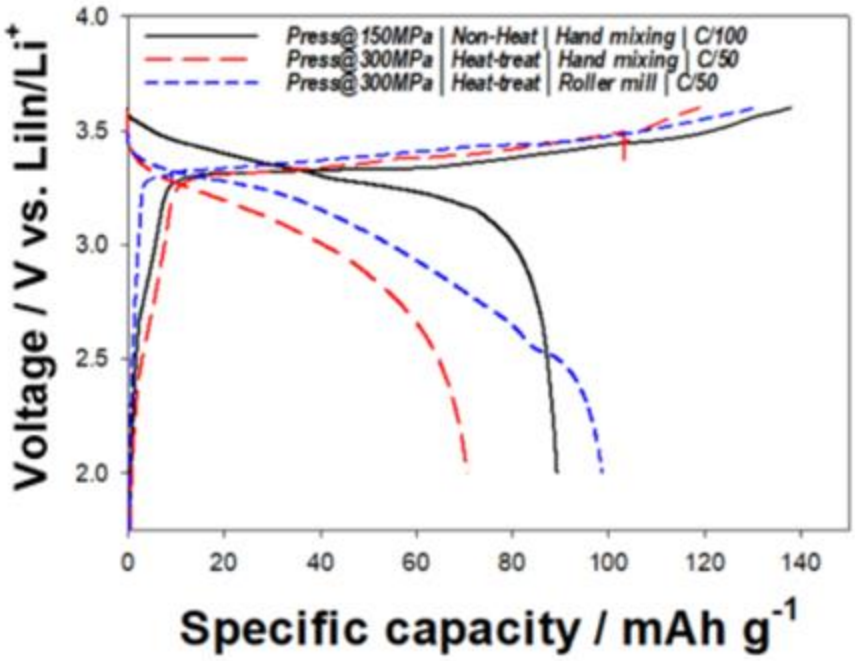

Figure 23: Initial charge-discharge data comparison between tests 3-5

Chapter 4: Conclusion

In conclusion, the new tool that I designed and fabricated can facilitate faster heat transfer to the battery compounds, withstand higher pressure on the battery compounds, and is a more compact design compared to the MTI tool seen in Figure 4 that I have chosen to benchmark. The heat transfer has been improved by decreasing the 0.889 inch wall thickness in the MTI PEEK plastic sleeve to a 0.5 inch wall thickness consisting of 0.375 inch 440c stainless steel and 0.125 inch PEEK plastic. The maximum pressure that can be exerted on the new tooling is around 303 MPa on the battery compounds while the MTI tool can only support 20 MPa, which correlates to 15.15 times more pressure. In addition to the higher pressure allowed, the new tool has a decreased outermost diameter and total assembly height. The more compact design will allow easier use

inside of the Argon-filled glovebox. Additionally, the tooling passed sealing validation so it can be taken out of the glovebox for cycling while using air sensitive materials. In regards to the testing, the battery compounds that should be used in the tool for optimization are 40 mg of the cathode material, 60:5:35 weight percent of $LiNbO_3$-coated $LiCoO_2$:Carbon Black:$Li_{10}GeP_2S_{12}$, 160 mg of $Li_{10}GeP_2S_{12}$ for the solid electrolyte, and 0.5 inch diameter coin punch of indium metal foil. To properly prepare the cathode material mixture, a roller mill should be used for at least 24 hours to ensure a homogenous mixture. The test procedure has been well established allowing for the external parameters to be varied using the pressure standardization in Table 2, as well as heating up to 200°C for 45 minutes. The optimization of the battery compounds and procedure has achieved a maximum open circuit voltage of 3.6 volts vs LiIn/Li^+ and a maximum specific capacity of 100 g/mAh for the first cycle.

Chapter 5: Future Work

For future work on this tooling and the characterization of the battery compounds chosen I have a few recommendations. First, I would suggest using the detailed drawings to fabricate a higher quantity of the design to allow for more testing iterations to be done at once. The cycling of the battery compounds can take a few weeks to complete as some cycles take anywhere from 20 hours to 100 hours. Secondly, I would suggest possibly creating another iteration of the design which incorporates the secondary pressure system that is needed to maintain the air-tight seal. Thirdly, I would recommend further cycling on the testing parameters in test 5 to see if the cyclability has improved with the more homogeneous composite cathode mixture. Lastly, I would suggest using the testing procedure and battery material amounts to further characterize the

compounds to make a better correlation between the pressure and heat used and the battery's performance.

Appendix A: Part Drawings

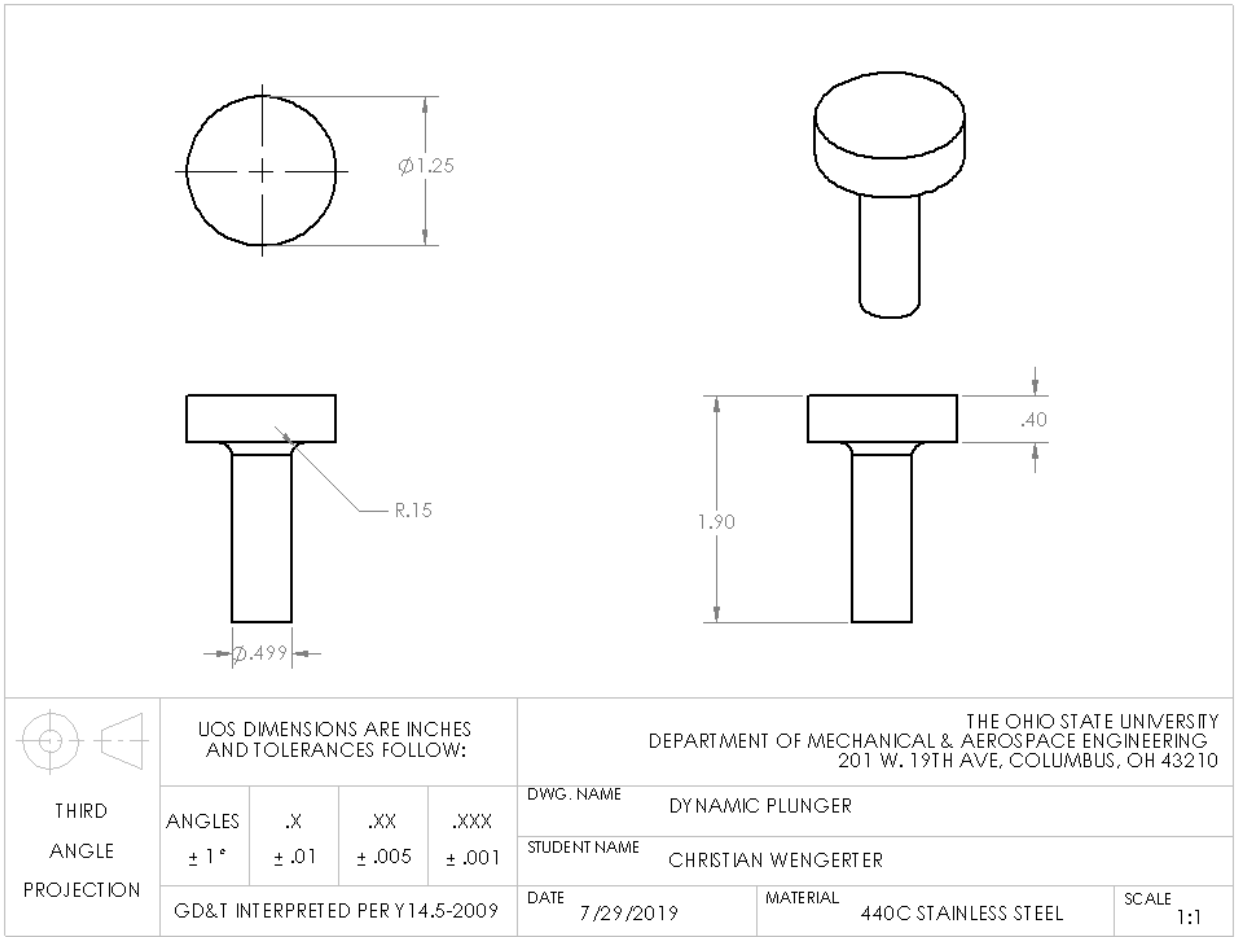

Figure 24: Dynamic plunger part drawing

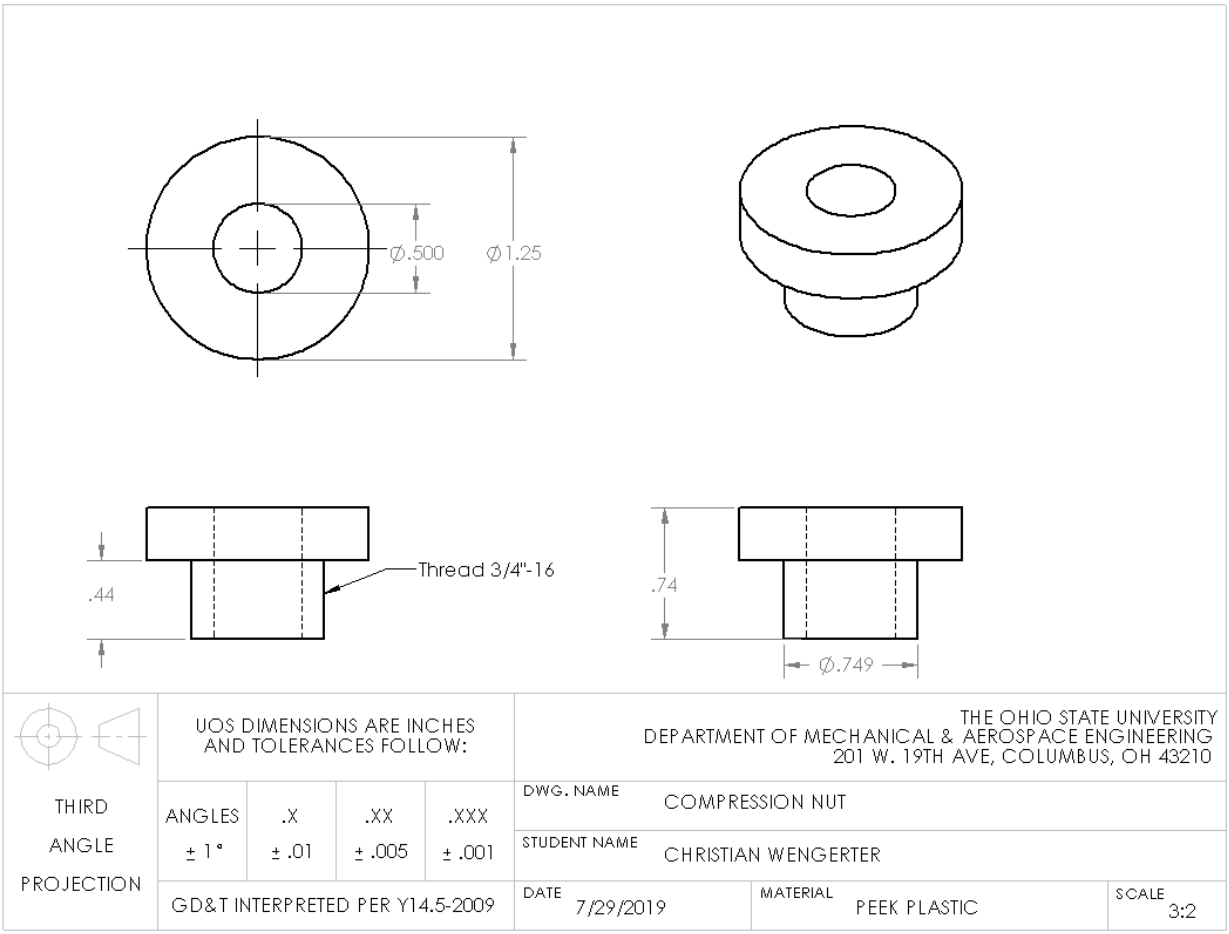

Figure 25: Compression nut part drawing

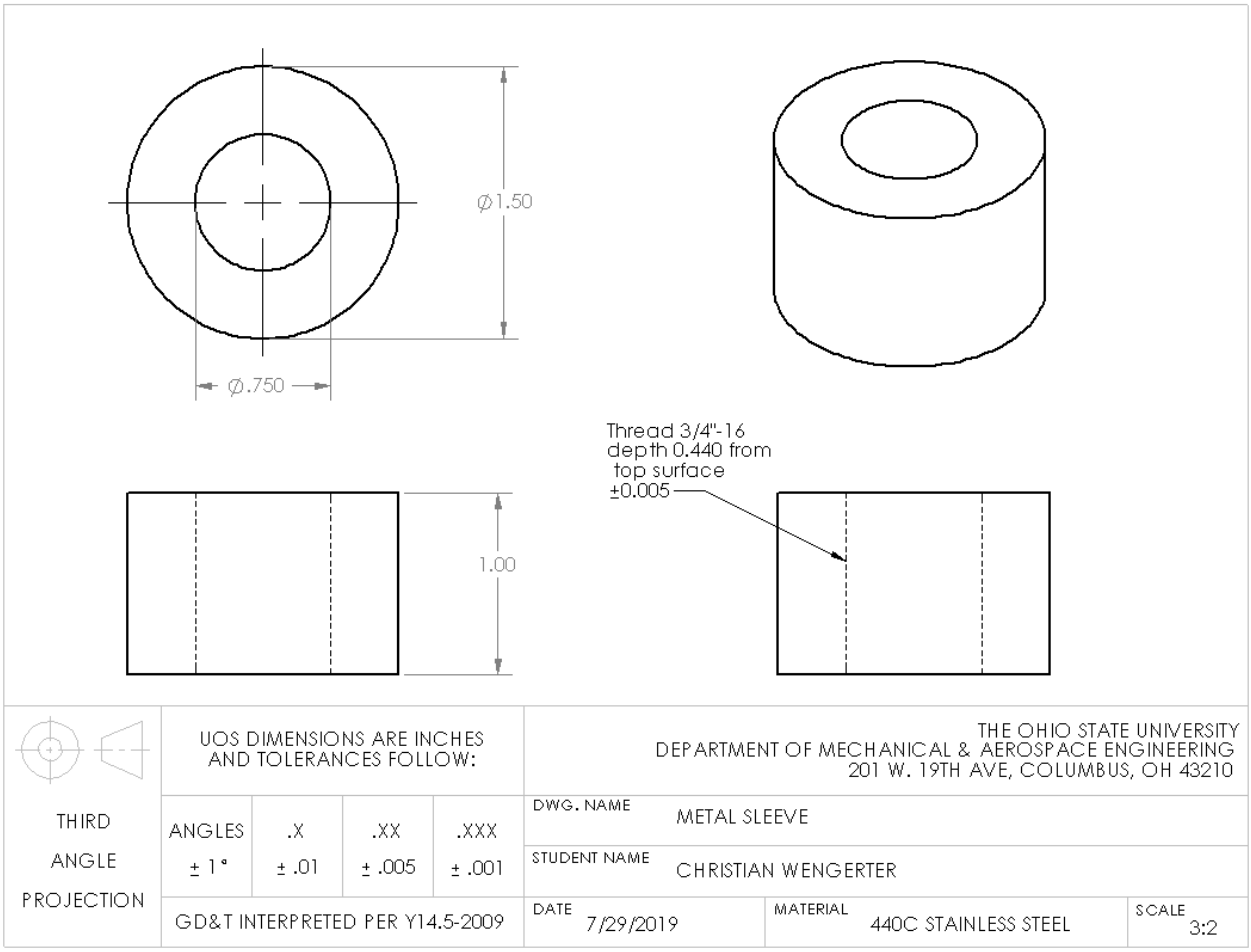

Figure 26: Metal sleeve part drawing

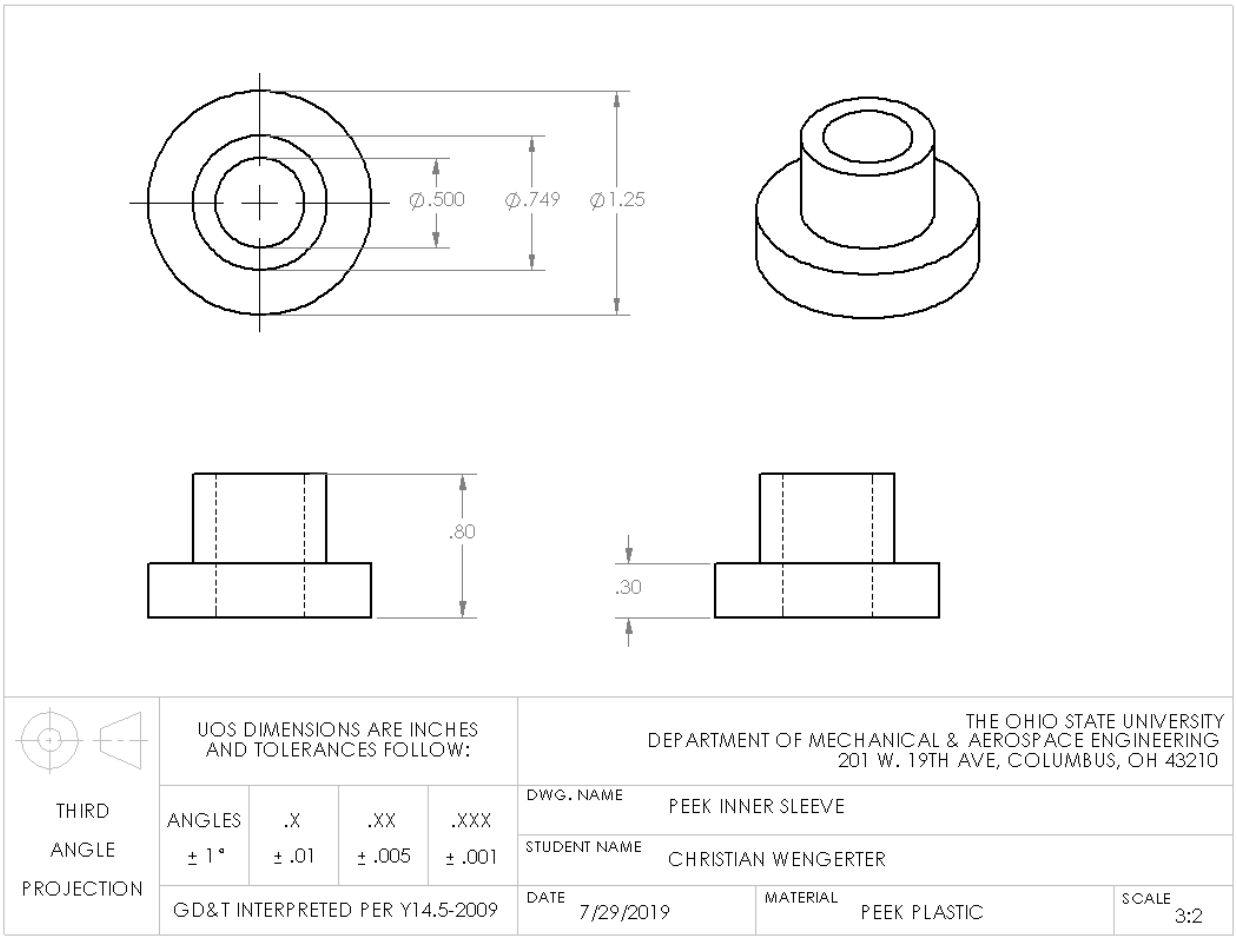

Figure 27: PEEK inner sleeve

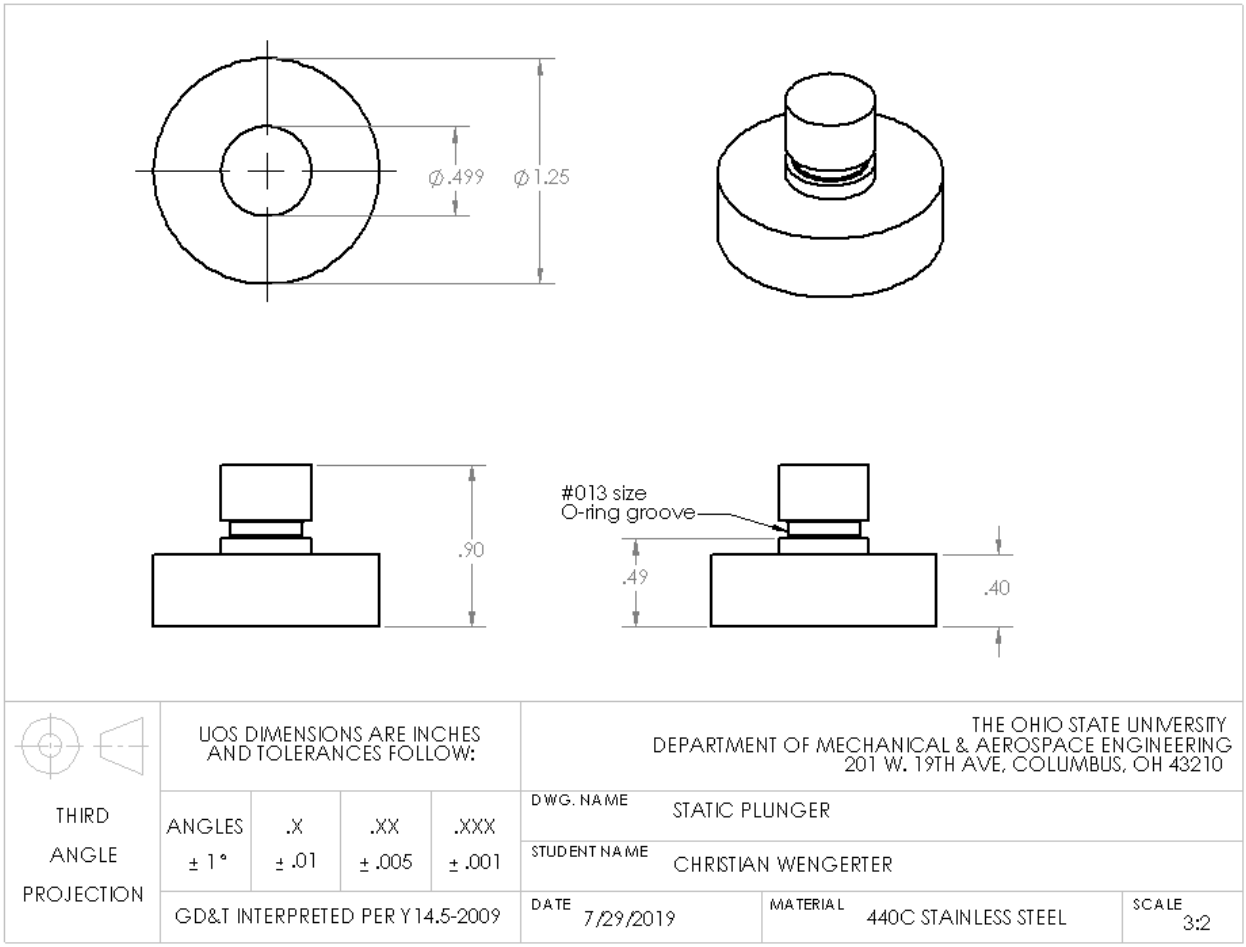

Figure 28: Static plunger part drawing

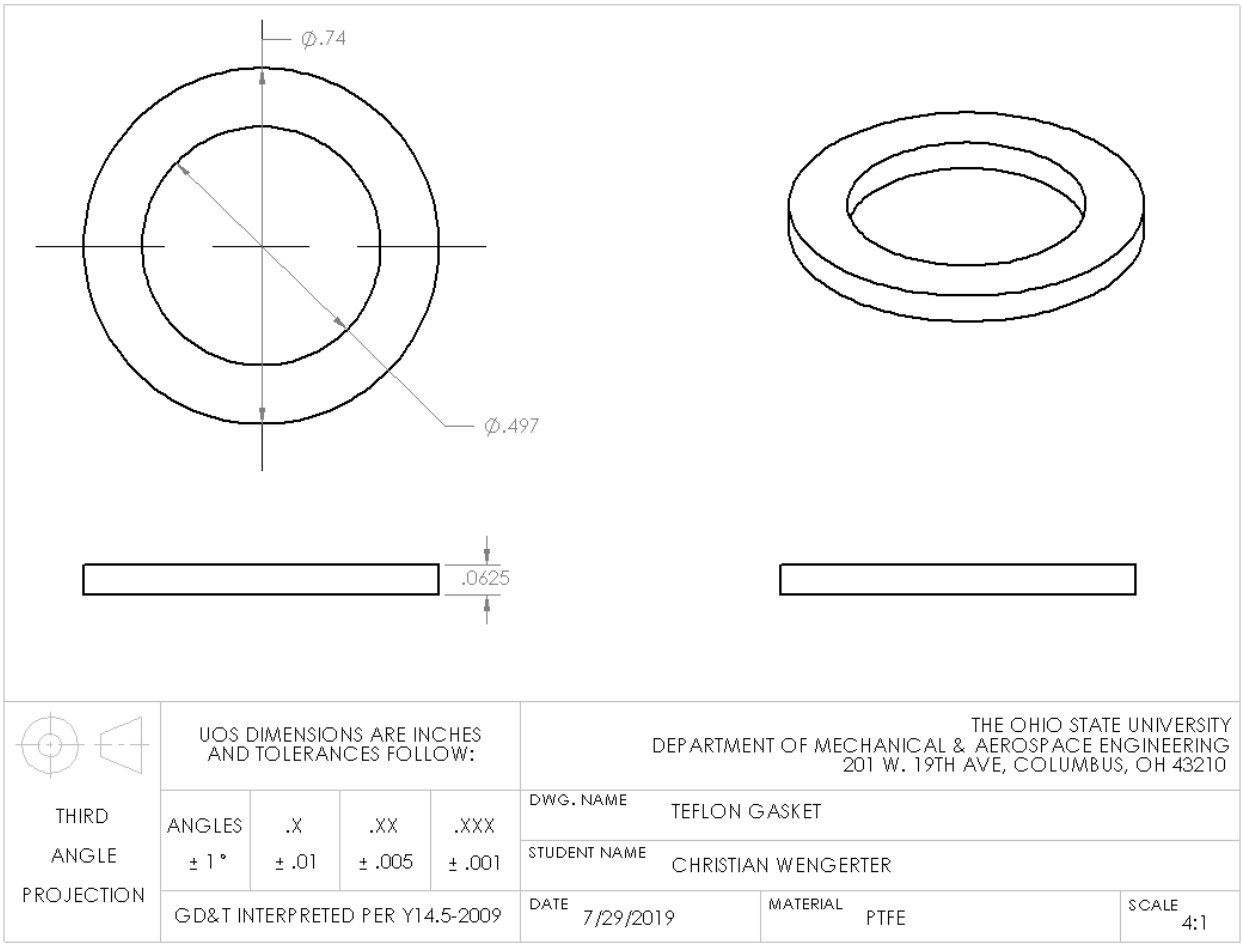

Figure 29: Custom Teflon gasket

Appendix B: Pressure Table Sample Calculation

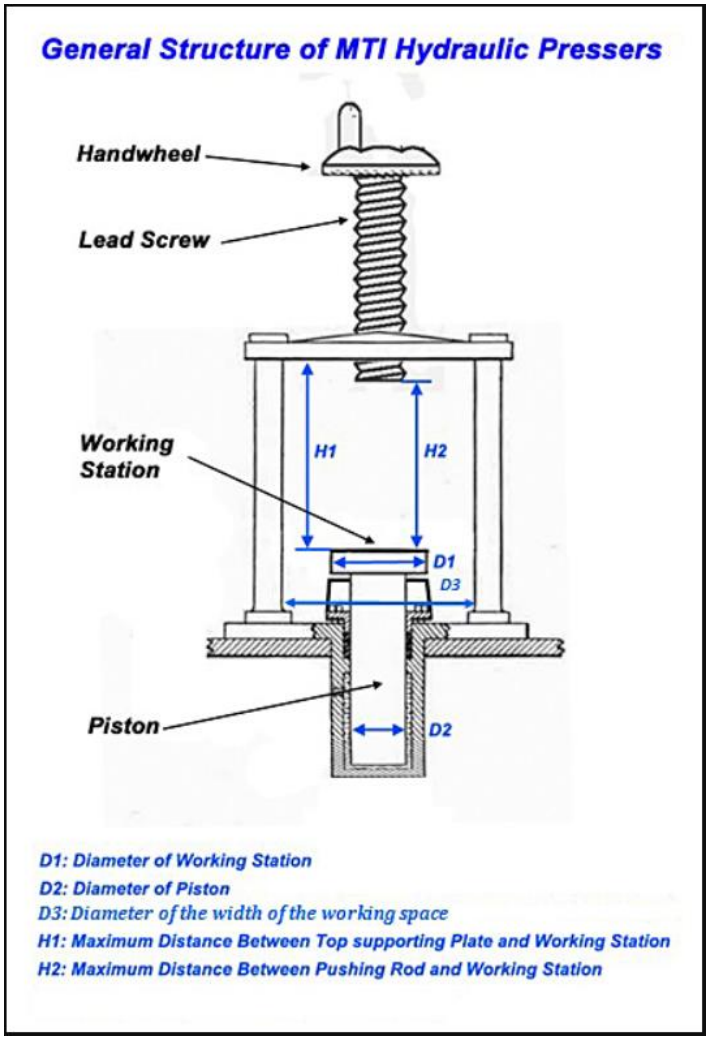

Figure 30: Schematic of hydraulic press from MTI Corp. [10]

Diameter used for hydraulic pressure gauge =D2= 70 mm

Inner diameter of new tool = 12.7 mm or 0.5 inch

$$Pressure = \frac{Force}{Area} \qquad \rightarrow \qquad Force = Pressure * Area$$

$$Force\ produced\ by\ hydraulic\ press = 10\ MPa\ * (\frac{1}{4} * \pi * (70mm)^2) = 38{,}484.51\ N$$

$$Pressure\ on\ battery\ compounds\ in\ new\ tool = \frac{(38484.51\ N)}{(\frac{1}{4} * \pi * (12.7mm)^2)} = 303.80\ MPa$$

References:

[1] J.-K. Park, Principles and Applications of Lithium Secondary Batteries, Wiley-VCH Verlag & Co., 2012.

[2] M. Tatsumisago, M. Nagao, A. Hayashi, Recent development of sulfide solid-electrolytes and interfacial modification for all-solid-state rechargeable lithium batteries, J. Asian Ceram. Soc. 1 (2013) 17–25. doi:10.1016/j.jascer.2013.03.005.

[3] J. Hobson, Could Solid-State Batteries Last A Lifetime?, Hackaday. (2015). https://hackaday.com/2015/08/25/could-solid-state-batteries-last-a-lifetime/ (accessed March 12, 2020).

[4] J.G. Kim, B. Son, S. Mukherjee, N. Schuppert, A. Bates, O. Kwon, M.J. Choi, H.Y. Chung, S. Park, A review of lithium and non-lithium based solid state batteries, J. Power Sources. 282 (2015) 299–322. doi:10.1016/j.jpowsour.2015.02.054.

[5] Pressure Controlled (up to 20 MPa) Split Coin Cell with Optional Sizes For Solid State Battery Research - EQ-PSC, MTI Corp - Leading Provider of Lab Equipments and Advanced Crystal Substrates. (n.d.). https://www.mtixtl.com/PEEKNylonSplitFlatCellforRandDBattery-Cell-PSC.aspx (accessed March 12, 2020).

[6] 440C Stainless Steel Plate - UNS S44004, United Performance Metals - Supplier of High Temperature Alloys. (n.d.). https://www.upmet.com/products/stainless-steel/440c (accessed March 16, 2020).

[7] S.R. Kim, D.H. Kim, D.J. Kim, M.H. Kim, J.M. Park, Study on Thermal Conductivity of Polyetheretherketone/Thermally Conductive Filler Composites, Solid State Phenomena Advances in Nanomaterials and Processing. (2007) 1079–1082. doi:10.4028/3-908451-31-0.1079.

[8] J.E. Shigley, C.R. Mischke, Standard handbook of machine design, McGraw-Hill, New York, 1996.

[9] W. Zhang, D.A. Weber, H. Weigand, T. Arlt, I. Manke, D. Schröder, R. Koerver, T. Leichtweiss, P. Hartmann, W.G. Zeier, J. Janek, Interfacial Processes and Influence of Composite Cathode Microstructure Controlling the Performance of All-Solid-State Lithium Batteries, ACS Appl. Mater. Interfaces. 9 (2017) 17835–17845. doi:10.1021/acsami.7b01137

[10] 15T Laboratory Press with built in Hydraulic Pump - YLJ-15L, MTI Corp - Leading Provider of Lab Equipments and Advanced Crystal Substrates. (n.d.). https://www.mtixtl.com/EQ-YLJ-15L.aspx (accessed March 12, 2020).

[11] K. Nakajima, T. Katoh, Y. Inda, B. Hoffman, Lithium ion conductive glass ceramics: properties and application in lithium metal batteries, in: Symp. Energy Storage Lithium Ion Mater. Perspect. Oak Ridge Natl. Lab. TN, 2010: pp. 7–8. http://www.ohara-inc.co.jp/cn/product/electronics/dl/OHARA%20Presentation%20140203.pdf (accessed July 10, 2015).

[12] V. Thangadurai, S. Narayanan, D. Pinzaru, Garnet-type solid-state fast Li ion conductors for Li batteries: critical review, Chem. Soc. Rev. 43 (2014) 4714–4727. doi:10.1039/C4CS00020J.